2018

Design for Microchannel Condensers with Separation Circuiting

Jun Li
ACRC, University of Illinois at Urbana-Champaign, United States of America, junli9@illinois.edu

Predrag S. Hrnjak
pega@illinois.edu

Design for Microchannel Condensers with Separation Circuiting

Jun LI[1], Pega HRNJAK[1,2]*

[1]ACRC Air Conditioning and Refrigeration Center
Department of Mechanical Science and Engineering,
University of Illinois at Urbana-Champaign
Urbana, IL, USA
junli9@illinois.edu

[2]Creative Thermal Solution
Urbana, IL, USA
pega@illinois.edu

* Corresponding Author

ABSTRACT

It has been proved both experimentally and by modeling that separation of vapor and liquid is beneficial for performance of a condenser prototype with a specific separation circuiting. The prototype has an inlet in the middle of the height and separates into two flow paths after the second header. The two paths recombine upstream of the exit of the condenser. This paper presents a search for optimal design for condensers with separation circuiting based on an experimentally validated steady-state condenser model. That model incorporates a mechanistic model of flow in header to calculate phase separation efficiency. Parametric studies are performed on pass circuitry, fin density and air velocity distribution. The trade-off between high heat transfer and high pressure drop for flow in the vapor path is further explained. After design optimization, the condenser with separation circuiting shows potential for 17.9% performance improvement compared to the baseline condenser with the same total air-side area.

1. INTRODUCTION

Modelling and optimization towards condensers for refrigeration and air conditioning systems is not a new topic. Heun and Dunn (1995) provided a systematic evalution of the effect of port shape on microchannel tube performance. On top of that, they carried out an analytical study to improve microchannel condenser design. Refrigerant-side circuiting and port shape significantly impacted the design. Kulkarni et al. (2001) optimized a sawtooth condenser for refrigerators. The optimal design was reached when the added condenser area caused so much pressure drop that the air flow rate dropped to the point where the air and refrigerant temperatures pinched. Using a more powerful and efficient fan was recommended to achieve further increases in condenser performance. Martinez-Ballester et al. (2013) presented a numerical model for microchannel condensers. Fin cuts was studied as a function of the refrigerant circuitry. Huang et al. (2015) explored the effect of variable geometry (fin depth, fin density, MC tube) on air cooled microchannel condensers using their established thermal system calculating platform. Capacity was plotted as a function of material mass for variable geometry and conventional geometry.

Li and Hrnjak (2017a) demonstrated the benefit of phase separation in header in condensers by modelling while assuming a certain degree of separation happens in the header. Phase separation will lower the refrigerant exit temperature by 1.3 K or increase the condensate flow by 6.1%. Different from a traditional multi-pass condenser which starts from the top and ends at the bottom, the separation condenser shown by Figure 1(a) is designed to have vapor-liquid separation in the vertical second header. After condensation in the 1st pass, the quality coming into the second header is 0.4-0.7 depending on working conditions. The generated liquid will separate from vapor due to larger density and higher viscosity. Based on the fact that high-quality, vapor-rich flow will have much higher heat transfer coefficient than liquid-rich flow, this design will give in-tube heat transfer enhancement shown by Figure 1(b). In this way, the heat transfer coefficient of the whole condenser is expected to be improved. The liquid-vapor separation in the second header, which is only based on header orientation and physical property difference, will provide almost

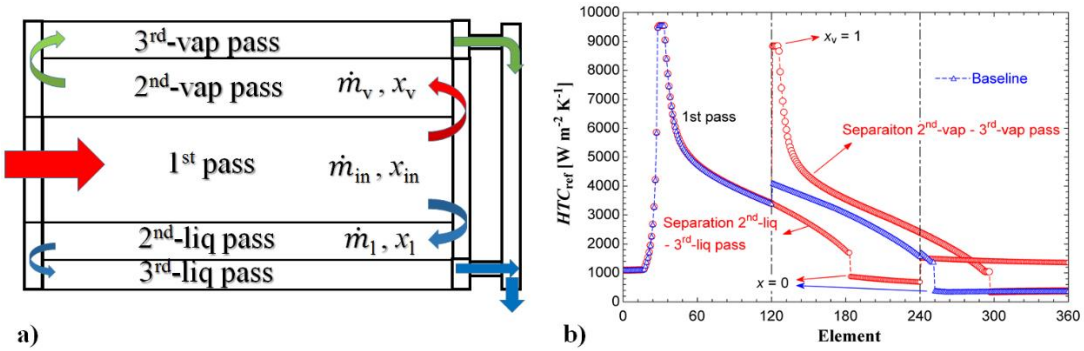

Figure 1: (a) Concept of separation in a parallel-flow condenser; (b) In-tube heat transfer enhancement of the separation condenser (Li and Hrnjak 2017a)

no additional cost for manufacturing.

Although Li and Hrnjak (2017a) showed the potential of separation condensers, the benefit was only indicated in one circuitry with fixed geometrical characteristics, e.g. pass circuitry, microchannel tube hydraulic diameter, width-height ratio, etc. Also, the quality going into the 2nd-vapor pass was pre-assumed: $x_v > x_{in}$ in Figure 1(a) – meaning phase separation happens. In other words, the separation efficiency was assumed.

Li and Hrnjak (2018) built a separation condenser model with a header model incorporated for calculating the separation efficiencies. This paper will use that condenser model to study the design of separation condensers. It is the goal of this paper to explore the effects of three design parameters: pass circuitry, fin density, and air flow distribution.

2. POTENTIAL OF SEPARATION CONDENSER

Two types of microchannel condensers in Figure 2 are compared in Li and Hrnjak (2017b) on a MAC system: Figure 2(a) is a 3-pass traditional baseline; Figure 2(b) is a 2V2LS (two vapor passes – two liquid passes – one subcooling pass) separation condenser. Both condensers are cross-flow, single-slab condensers with louver fins. Each has 54 MC tubes and only the circuitries for passes are different. Number of microchannel tubes is shown on each pass in Figure 2. The other geometries for the two condensers are kept the same such as length, height, fin geometries, microchannels,

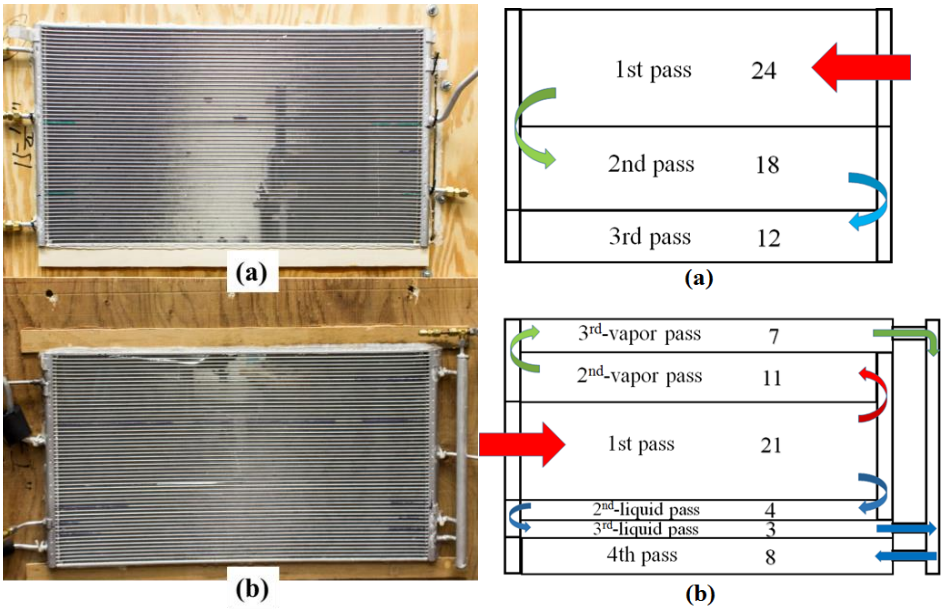

Figure 2: Condensers for comparison in Li and Hrnjak (2017b): (a) Baseline condenser; (b) Separation condenser

headers, etc. Two condensers are identical on the air side each with a total face area of 0.275 m^2, core depth of 12 mm and a total air-side heat transfer area of 5.22 m^2. Table 1 presents the main geometry for simulated condensers.

The first criterion for evaluating a condenser is the refrigerant exit temperature T_{cro}. In experiments, inlet temperature T_{cri}, refrigerant mass flow rate $\dot{m}_{ref}$ and condensing temperature T_{cd} are controlled to be the same. A more effective condenser should condense the same flow rate of refrigerant to a lower temperature (T_{cro}) providing the same air conditions. T_{cd} is determined from condensing pressure which is taken as the average of the inlet pressure and exit pressure.

Comparison is done at two air conditions per SAE Standard J2765 (2008) and results are in Figure 3. It is found by experiments that separation condenser constantly has a lower exit temperature T_{cro} than the baseline condenser for the same air side flow rate and temperature. The biggest difference on T_{cro} between baseline condenser and separation condenser from modeling is 0.9 K at M35a. Although separation condenser condenses the refrigerant to a lower exit temperature, condenser capacity is not improved drastically in this kind of comparison. The reason is that the bigger subcooling will bring about bigger subcooling region which will not help a lot on heat transfer, especially when refrigerant exit temperature already approaches the air ambient temperature. Larger improvement should be expected for comparison at reduced degree of subcooling.

So, the second comparison criterion is the condensate flow rate. A more effective condenser condenses more

Table 1: Main geometries of the MAC microchannel condenser with separation circuiting

Item	Value	Item	Value
Width w/ headers [mm]	710	Number of MC ports per tube [-]	12
Width w/o headers [mm]	680	Fin thickness [mm]	0.1
Width covered by fin [mm]	670	Fin pitch [mm]	1.21
Height w/ side plates [mm]	405	Louver pitch [mm]	0.88
Height w/o side plates [mm]	390	Louver length [mm]	4.0
Depth [mm]	12.2	Louver angle [-]	28
MC tube thickness [mm]	1.43	Header type	D-shape
MC tube pitch [mm]	7.0	Header equivalent diameter [mm]	11.0
MC port D_h [mm]	0.66		

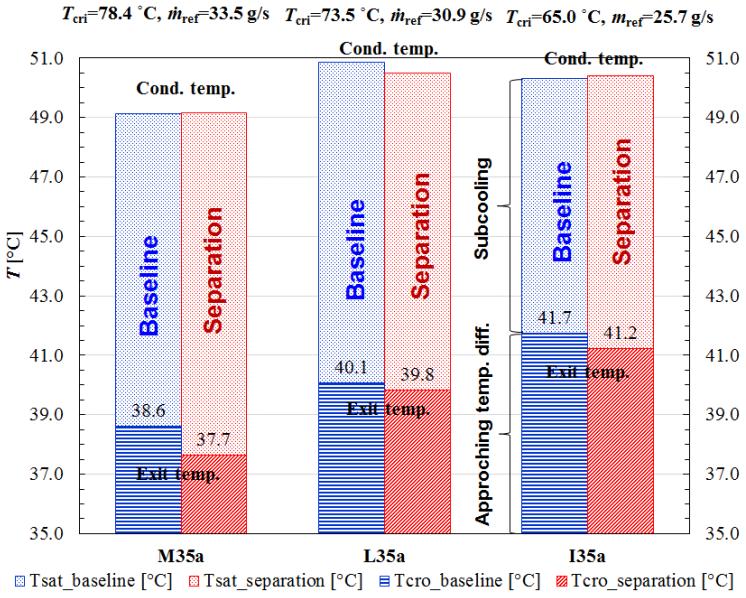

Figure 3: Exit temperature T_{cro} (numbers in the bars) and condensing temperature T_{cd} (top of the bars) for the two condensers at the same $\dot{m}_{ref}$ and T_{cri}, three SAE operating conditions

refrigerant. For the two condensers, air-side conditions are again kept the same with the first comparison. On refrigerant side, T_{cri}, T_{cro}, and T_{cd} should be controlled the same between the two condensers. Subcooling is ensured throughout the test conditions.

For each simulated case of T_{cri} and T_{cro}, Figure 4 shows the separation condenser constantly condenses more refrigerant than the baseline for the same air side flow rate and temperature. The mass flow rate improvement varies from 1.6% to 7.4% in tested conditions. For M35a, even though with a slightly smaller refrigerant-air *LMTD*, the benefit of higher *UA* dominates the drawback of smaller *LMTD*, so separation condenser ends up with a 5.1% increase on capacity.

This paper first uses the same geometry of the separation condenser (Table 1) but varies condenser pass circuitry to achieve an optimization of separation condenser design. Similar condenser comparison criteria will be used. On top of that, fin density and air-side free face velocity will then be altered to explore their effect on the design. Operating condition of the separation condenser is going to be kept the same with M35a in Figure 3, as shown in Table 2.

The simulation and property evaluations are carried out in MATLAB (R2017a). Refrigerant properties are calculated from REFPROP 8.0 (NIST, 2007). The number of element in each microchannel tube is chosen to be 120. Further increment of the element number will not cause the subcooling to vary over ± 0.03 K, and the resulting change on capacity is under 0.1%.

2. PASS CIRCUITRY

Under the same inlet conditions (P_{cri} and T_{cri}), air side conditions, and refrigerant mass flow rate $\dot{m}_{ref}$, subcooling is used as the criterion for judging condenser performance. The bigger the subcooling is, the more effective is the condenser.

In order to quantify the separation performance of the header, two separation efficiencies are defined. According to the notation in Figure 1, liquid separation efficiency is defined as the ratio of separated liquid which flows into the 2nd-liquid pass to the liquid supplied to the inlet. Similarly, vapor separation efficiency is evaluated as the ratio of the

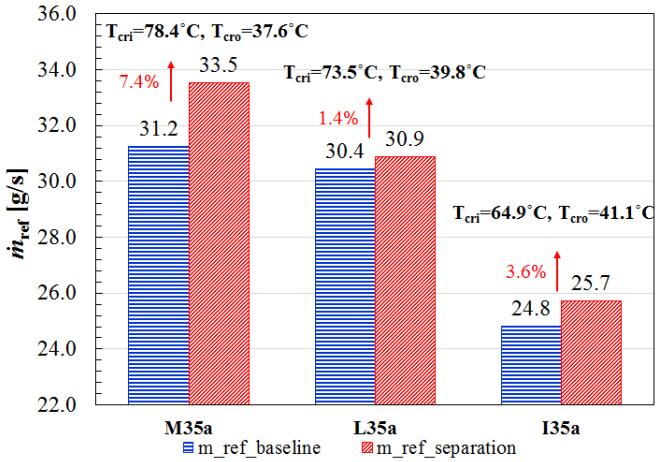

Figure 4: Mass flow rate $\dot{m}_{ref}$ for the two condensers at the same T_{cri} and T_{cro}, at three operating conditions

Table 2: Simulated inlet condition for R134a

Parameter	Value
P_{cri} [kPa]	1329
T_{cri} [°C]	78.4
T_{cai} [°C]	35.1
V_{cai} [m/s]	3.03
RH_{cai} [-]	15%
$\dot{m}_{ref}$ [g/s]	33.5

separated vapor which flows into the 2nd-vapor pass to the total amount of vapor entering the header:

$$\eta_{\mathrm{l}} = \frac{\dot{m}_{\mathrm{l,l}}}{\dot{m}_{\mathrm{l,v}} + \dot{m}_{\mathrm{l,l}}} \tag{1}$$

$$\eta_{\mathrm{v}} = \frac{\dot{m}_{\mathrm{v,v}}}{\dot{m}_{\mathrm{v,v}} + \dot{m}_{\mathrm{v,l}}} \tag{2}$$

where $\dot{m}_{\mathrm{v,v}}$ and $\dot{m}_{\mathrm{l,v}}$ are the vapor mass flow rate and liquid mass flow rate, respectively, at the vapor exit; $\dot{m}_{\mathrm{v,l}}$ and $\dot{m}_{\mathrm{l,l}}$ are the vapor mass flow rate and liquid mass flow rate, respectively, at the liquid exit.

310 simulated condenser circuitings have been simulated. When assigning tube number to each pass, the number of tubes for passes should decrease as condensate is formed. These rules on circuitry work as the bottom line when working out the optimal circuitry. Table 3 lists the 20 ranks in those simulations. The total tube number remains 54. Two adjacent ranks are differentiated by the difference of subcooling of the modeling accuracy 0.06 K. Each circuiting is named by the tube number array $N_{1\mathrm{st}}$-$N_{2\mathrm{v}}$-$N_{2\mathrm{l}}$-$N_{3\mathrm{v}}$-$N_{3\mathrm{l}}$-$N_{4\mathrm{th}}$ (for example, 23-11-5-5-3-7).

Since the move of one or two tubes would cause very little impact on subcooling, One rank may have several circuitings that generate a subcooling within ±0.03 K. Inlet quality to the second header $x_{1\mathrm{st,ro}}$ and the qualities into the 2nd-vapor pass and 2nd-liquid pass are also listed in Table 3. It shows that phase separation indeed happens in the second header, but not complete, indicated by η_{v} and η_{l}. Basically, liquid entrainment to the 2nd-vap pass would cause the $x_{2\mathrm{v,ri}}$ to drop. $x_{2\mathrm{v,ri}}$ is generally bigger than $x_{1\mathrm{st,ro}}$ by 0.1 – 0.3, while $x_{2\mathrm{l,ri}}$ smaller than $x_{1\mathrm{st,ro}}$ by 0.1 – 0.3.

It is worth noting that the original 2V2LS design (21-11-7-4-3-8) in the experiments in Li and Hrnjak (2017b) has a subcooling 10.70 K, which is at the ninth rank in Table 3.

For the top ranks, subcooling is not sensitive to change of circuitry. Just for the first rank, there are 25 circuitings. Table 4 reveals that the top 20 of them. In fact, since the Top 20 listed out in Table 4 have the biggest difference within the modelling accuracy 0.06 K difference, they can all be regarded as the best circuitings. It can be found that, to achieve the optimal subcooling for the 2V2LS condenser, $N_{1\mathrm{st}}$ will need to be 25 or 26, which is a bit less (1 – 2 tubes)

Table 3: Overall look of 20 ranks for 2V2LS condensers

Circuiting	Subcooling [K]	$x_{1\mathrm{st,ro}}$	$x_{2\mathrm{v,ri}}$	$x_{2\mathrm{l,ri}}$	η_{v}	η_{l}
25-9-4-6-3-7	11.16	0.460	0.606	0.313	0.660	0.636
26-8-3-7-3-7	11.10	0.435	0.608	0.303	0.603	0.704
23-12-5-4-3-7	11.04	0.512	0.621	0.325	0.768	0.504
23-4-2-13-7-5	10.98	0.512	0.743	0.459	0.267	0.909
27-8-6-4-3-6	10.92	0.409	0.560	0.218	0.764	0.585
23-10-7-4-3-7	10.86	0.512	0.621	0.329	0.764	0.504
26-15-3-3-2-5	10.80	0.435	0.566	0.182	0.858	0.492
21-6-5-10-4-8	10.74	0.565	0.721	0.474	0.469	0.767
24-11-3-7-2-7	10.69	0.486	0.632	0.320	0.691	0.621
24-13-3-3-3-8	10.62	0.486	0.609	0.276	0.788	0.525
25-7-7-4-3-8	10.56	0.460	0.613	0.274	0.731	0.608
18-14-5-6-3-8	10.50	0.646	0.720	0.520	0.700	0.506
21-16-6-4-3-4	10.44	0.565	0.650	0.366	0.810	0.429
30-6-5-3-2-8	10.38	0.335	0.494	0.140	0.812	0.580
26-16-3-3-2-4	10.32	0.435	0.563	0.180	0.859	0.492
22-4-3-13-8-4	10.24	0.539	0.763	0.483	0.275	0.905
19-10-7-5-5-8	10.18	0.619	0.705	0.491	0.675	0.547
23-3-2-9-7-10	10.11	0.512	0.754	0.455	0.278	0.909
23-3-2-12-10-4	10.07	0.512	0.804	0.464	0.227	0.939
23-4-3-7-7-10	9.83	0.512	0.683	0.442	0.383	0.817

Table 4: Top 20 circuitings for 2V2LS condenser

Circuiting	Subcooling [K]	$x_{ro,1st}$	$x_{ri,2v}$	$x_{ri,2l}$	η_v	η_l
25-9-4-6-3-7	11.162	0.460	0.606	0.313	0.660	0.636
25-10-3-6-3-7	11.161	0.460	0.609	0.318	0.653	0.636
24-10-4-6-3-7	11.160	0.486	0.622	0.335	0.669	0.621
26-10-4-5-3-6	11.158	0.435	0.582	0.261	0.726	0.596
26-10-3-6-3-6	11.144	0.435	0.595	0.278	0.675	0.650
24-12-4-5-3-6	11.139	0.486	0.621	0.300	0.737	0.579
25-10-4-5-3-7	11.138	0.460	0.609	0.288	0.712	0.608
26-11-3-5-3-6	11.138	0.435	0.593	0.256	0.721	0.623
26-9-4-5-3-7	11.137	0.435	0.585	0.270	0.701	0.623
24-9-4-7-3-7	11.137	0.486	0.631	0.352	0.627	0.650
24-11-4-5-3-7	11.135	0.486	0.617	0.318	0.715	0.579
26-8-4-6-3-7	11.134	0.435	0.590	0.293	0.649	0.650
26-10-3-5-3-7	11.133	0.435	0.587	0.275	0.693	0.623
25-10-4-6-3-6	11.130	0.460	0.615	0.292	0.692	0.636
25-12-4-4-3-6	11.128	0.460	0.590	0.261	0.777	0.540
24-12-3-6-3-6	11.127	0.486	0.627	0.326	0.683	0.621
24-11-4-6-3-6	11.126	0.486	0.632	0.315	0.698	0.621
25-8-4-7-3-7	11.122	0.460	0.613	0.331	0.615	0.664
26-11-4-4-3-6	11.120	0.435	0.581	0.230	0.779	0.569
25-11-3-5-3-7	11.118	0.460	0.606	0.296	0.700	0.608

than half of the total tube number. Then the tube number for each pass generally follows the order $N_{2v} \geq N_{2l} \geq N_{3v}, N_{3l}$. N_{4th} will be 7 or 6.

Li and Hrnjak (2016) have shown that higher separation efficiency in the second header does not necessarily benefit the condenser performance. The reason for that, as indicated by Li and Hrnjak (2017a), is the trade-off between high heat transfer coefficient and large pressure gradient of vapor flow in the vapor path. In a separation condenser, the upper vapor path and the lower liquid path would finally mix in an integrated receiver. Pressure drop through vapor path and through liquid path must equalize. More vapor going into the vapor path will make the pressure drop higher thus the vapor amount (mass flux) is limited. Lower mass flux will cause lower heat transfer coefficient.

With higher quality x_v (equivalent to higher separation efficiency) entering the vapor path, the mass flow rate $\dot{m}_v$ in the vapor path should drop. From Cavallini et al. (2006):

$$\left(dp/dz\right)_f = \phi_{lo}^{\ 2} \frac{2 f_{lo} G^2}{D_h \rho_l} \tag{3}$$

where $f_{lo}=0.046Re^{-0.2}$ and Φ_{lo}^2 is a curve-fitting constant based on quality x. Φ_{lo}^2 generally increases with x and reaches peak around x=0.9. So $(dp/dz)_f \propto G^{1.8}$. Since the axial length z is independent of G, the pressure drop in flow path $dp \propto G^{1.8}$. From Figure 5, it is evident that the *HTC* must have smaller exponentiation with respect to G than $(dp/dz)_f$ does. So, to compensate the deterioration of *HTC* due to dp constraint, the relative heat transfer area of the vapor path with respect to the liquid path appears to be important. If this relative quantity can be manipulated well, the condenser capacity should have monotonical relationship with separation efficiency.

3. FIN DENSITY

Based on the analysis in Section 2, we want to increase the heat transfer area of the vapor path to compensate the higher pressure drop of vapor-rich flow. More MC tube can increase the area but cannot maintain the mass flux. The other solution would be to increase the fin-side area. Thus, as illustrated by Figure 6, fin density in the vapor path will be increased in this section. To maintain the material cost the same, fin density in the liquid path will be decreased. The fin densities in the first pass and in the fourth pass stay the same. Thus, the total fin number will stay the same.

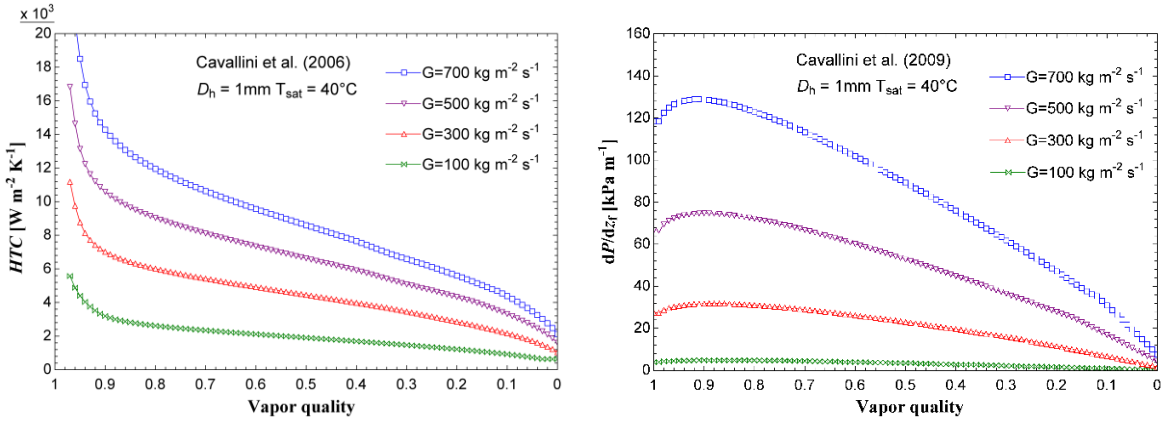

Figure 5: R-134a in a 1mm smooth tube at T_{sat}=40 °C: (a) Heat transfer coefficient (Cavallini et al., 2006); (b) Frictional pressure gradient (Cavallini et al., 2009)

Air velocity can be controlled by grille or fan arrays, so it is assumed to be uniform (3.0 m/s) as in Section 2.

The top five designs in Table 4 are picked out as the baseline to check the improvement. The uniform fin pitch is 1.21 mm in Table 1 and the length of a tube covered by fins is 670 mm. For uniform fin pitch, there are 554 fins per row and 12182 fins for the vapor path and liquid path. The variable fin density is shown in Table 5. Fin pitch in the vapor path and that in the liquid path are shown in pair with one increasing and the other decreasing.

Figure 7 demonstrates that for each of the circuiting, changing fin density will alter the subcooling. Pair 4 (609 fins per row in vapor path and 468 fins per row in the liquid path) gives the biggest subcooling. The maximum increase of subcooling happens at 26-10-4-5-3-6 using Pair 4. Its subcooling is 11.24 K, bigger than the 11.16 K of the uniform density baseline by more than the modelling accuracy. This is an improvement by one rank from Table 3.

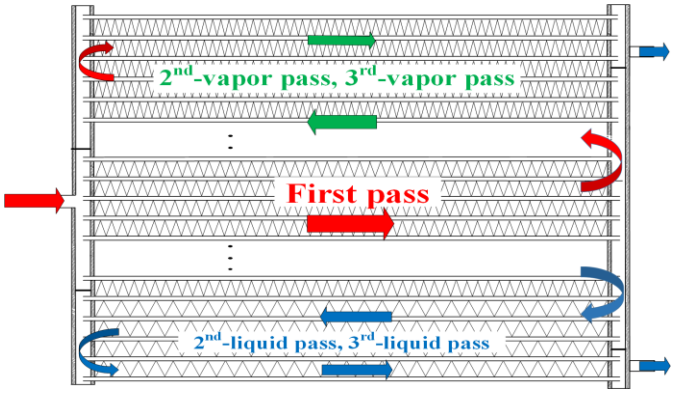

Figure 6: Varying fin density in vapor path and liquid path of the separation condenser

Table 5: Variable fin pitches for the vapor path and the liquid path

Circuiting	Pair 1	Pair 2	Pair 3	Pair 4	Pair 5	Pair 6	Pair 7
25-9-4-6-3-7	0.9 / 2.4	1 / 1.74	1.05 / 1.55	1.1 / 1.41	1.15 / 1.31	1.25 / 1.16	1.3 / 1.1
25-10-3-6-3-7	0.9 / 2.4	1 / 1.74	1.05 / 1.55	1.1 / 1.41	1.15 / 1.31	1.25 / 1.16	1.3 / 1.1
24-10-4-6-3-7	0.9 / 2.61	1 / 1.80	1.05 / 1.59	1.1 / 1.43	1.15 / 1.32	1.25 / 1.15	1.3 / 1.09
26-10-4-5-3-6	0.9 / 3.05	1 / 1.91	1.05 / 1.65	1.1 / 1.47	1.15 / 1.33	1.25 / 1.15	1.3 / 1.08
26-10-3-6-3-6	0.9 / 2.4	1 / 1.74	1.05 / 1.55	1.1 / 1.41	1.15 / 1.31	1.25 / 1.16	1.3 / 1.1

Vapor path fin pitch (mm) / Liquid path fin pitch (mm)

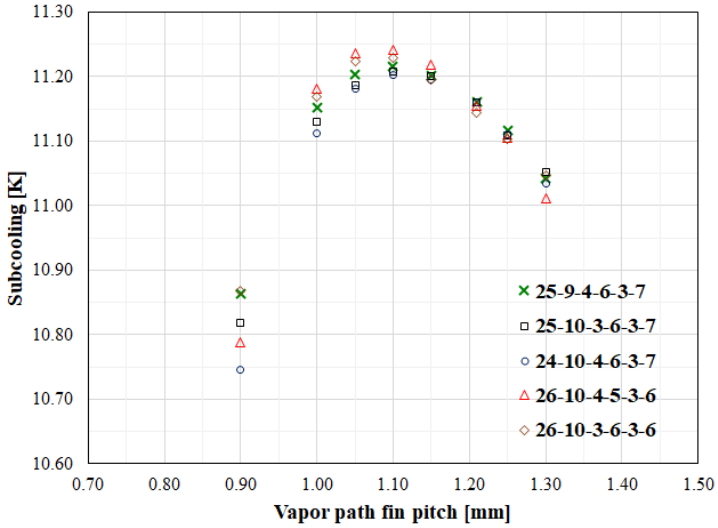

Figure 7: Subcooling for variable fin density in the separation condenser

4. AIR DISTRIBUTION

To maximize the condenser performance, we can give higher air velocity to passes with higher in-tube heat transfer coefficient. Other than the air side geometry, air load also affects the downstream flow resistance. In reality for a MAC system, there are many factors that could cause air velocity nonuniformity either passively or actively, such as bumper, fender, grille, fan number, fan position, condenser orientation, etc. It is worthwhile to explore the condenser sensitivity to pre-assumed air distribution as a first step towards understanding the design of separation condensers. Final design should take into account the on-site air velocity distribution.

Pair 4 of the five circuiting in Table 5 is chosen to check the improvement. The variable air velocity is shown in Table 6. Air velocity in the vapor path and that in the liquid path are shown in pair with one increasing and the other decreasing. The total air volumetric flow rate is controlled to be the same.

It can be demonstrated by Figure 8 that for each optimal-fin-density option of the five circuitings, air maldistribution will alter the subcooling. Again, 26-10-4-5-3-6 gives the biggest subcooling improvement. The biggest subcooling happens at Pair 6 of the air velocity. Its subcooling is 11.33 K, bigger than the 11.24 K of the uniform air velocity baseline by one more rank. Compared with 10.7 K of the baseline separation condenser (21-11-7-4-3-8), it is 0.63 K higher. Conclusion can be drawn that fin density and air velocity modification works better for separation condensers with higher area ratio of the vapor path to the liquid path.

26-10-4-5-3-6 with Pair 4 for fin density and Pair 6 for air velocity is taken to compare with two condensers (baseline separation condenser 21-11-7-4-3-8 and conventional condenser 24-18-12) from Li and Hrnjak (2017b). The comparison criterion is the condensate flow rate while controlling the inlet conditions and the outlet temperature T_{cro} to be the same. Three cases for T_{cro} are simulated shown in Figure 9. The inlet temperature and inlet pressure are the same as in Table 2. For each condenser, the mass flow rate is varied to achieve different outlet temperature T_{cro}.

Table 6: Variable air velocity for the vapor path and the liquid path

Circuiting	Pair 1	Pair 2	Pair 3	Pair 4	Pair 5	Pair 6	Pair 7	Pair 8
25-9-4-6-3-7	2.4 / 3.94	2.6 / 3.65	2.8 / 3.36	3.03 / 3.03	3.2 / 2.78	3.4 / 2.49	3.6 / 2.2	3.8 / 1.92
25-10-3-6-3-7	2.4 / 3.94	2.6 / 3.65	2.8 / 3.36	3.03 / 3.03	3.2 / 2.78	3.4 / 2.49	3.6 / 2.2	3.8 / 1.92
24-10-4-6-3-7	2.4 / 4.01	2.6 / 3.70	2.8 / 3.39	3.03 / 3.03	3.2 / 2.76	3.4 / 2.45	3.6 / 2.14	3.8 / 1.83
26-10-4-5-3-6	2.4 / 4.13	2.6 / 3.78	2.8 / 3.43	3.03 / 3.03	3.2 / 2.73	3.4 / 2.38	3.6 / 2.03	3.8 / 1.68
26-10-3-6-3-6	2.4 / 3.94	2.6 / 3.65	2.8 / 3.36	3.03 / 3.03	3.2 / 2.78	3.4 / 2.49	3.6 / 2.2	3.8 / 1.92

Vapor path air velocity (m/s) / Liquid path air velocity (m/s)

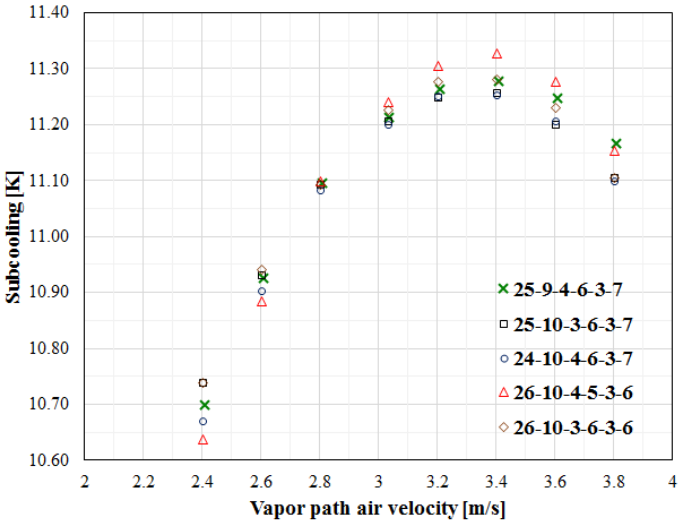

Figure 8: Subcooling for varying air velocity

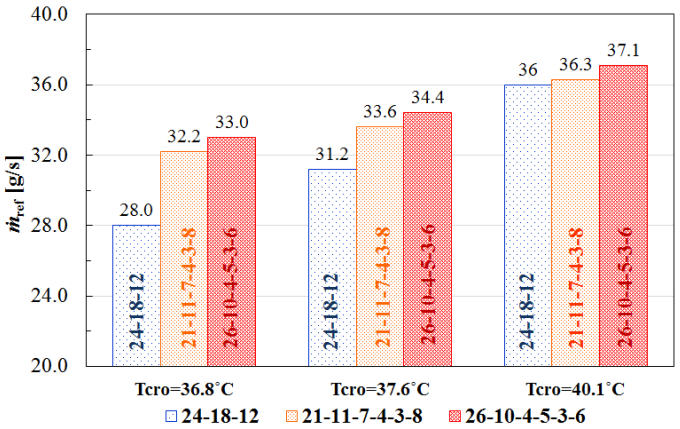

Figure 9: Comparison of condensate flow rate at the same inlet conditions and exit temperature T_{cro}

The order for the condensate mass flow rate $\dot{m}_{ref}$ is 26-10-4-5-3-6 > 21-11-7-4-3-8 > 24-18-12. At the same T_{cro}, pressure drop of the 26-10-4-5-3-6 separation condenser is bigger than that of the conventional condenser. However, in the subcooling region, outlet enthalpy is almost only a function of outlet temperature. Therefore, the specific enthalpy difference would be the same, then $\dot{m}_{ref}$ can manifest the magnitude of capacity. At the highest subcooling (T_{cro} = 36.8 °C), the 26-10-4-5-3-6 design with variable geometry and air velocity has about twice of the pressure drop of the conventional condenser, but it achieves 17.9% more condensate flow rate than the conventional condenser and 2.5% more than the 21-11-7-4-3-8 design.

5. CONCLUSION

This paper presents a search for optimal design for condensers with separation circuiting based on an experimentally validated steady-state condenser model. That model incorporates a mechanistic model of flow in header to consider phase separation efficiency. The trade-off between high heat transfer and high pressure drop for flow in the vapor path limits the performance improvement.

Parametric studies are performed on pass circuitry, fin density and air velocity distribution. Fin density and air velocity modifications work better for separation condensers with higher area ratio of the vapor path to the liquid path. Subcooling of the optimal separation condenser (26-10-4-5-3-6) with variable fin density and air distribution is bigger than that of the original separation condenser (21-11-7-4-3-8) by 0.63 K, when the original design has a subcooling of 10.7 K.

Use the condensate flow rate criterion and compare the optimal separation condenser with variable fin density and air distribution vs. the conventional condenser from Li and Hrnjak (2017b), the optimal design shows 17.9% increase of condensate flow than the conventional condenser. The optimal design might not be the final one though considering many causes for nonuniformity of air flow. The one applied in reality has to take into account the real air velocity distribution.

NOMENCLATURE

A	heat transfer area	(m^2)	**Subscripts**	
D	diameter	(m)	1st	1st pass
HTC	heat transfer coefficient	(W/m^2-K)	2v	2nd-vapor pass
$LMTD$	logarithm mean temperature difference	(K)	2l	2nd-liquid pass
$\dot{m}$	mass flow rate	(g/s)	3v	3rd-vapor pass
MAC	mobile air conditioning		3l	3rd-liquid pass
MC	microchannel		4th	4th pass
MCHE	microchannel heat exchanger		cd	condensing
N	number of tubes	(-)	cri	condenser refrigerant inlet
P	pressure	(kPa)	cro	condenser refrigerant outlet
Q	capacity	(kW)	in	inlet
RH	relative humidity	(-)	l (1st)	liquid phase
T	temperature	(°C)	l (2nd)	liquid path
UA	heat conductance	(W/K)	ref	refrigerant
x	vapor quality		ri	refrigerant inlet
Greeks			v (1st)	vapor phase
η	separation efficiency	(-)	v (2nd)	vapor path

REFERENCES

Cavallini, A., Doretti, L., Matkovic, M., & Rossetto, L. (2006). Update on Condensation Heat Transfer and Pressure Drop inside Minichannels. *Heat Transfer Engineering* 27(4),74–87.

Cavallini, A., Del Col, D., Matkovic, M., & Rossetto, L. (2009). Frictional Pressure Drop During Vapour–Liquid Flow in Minichannels: Modelling and Experimental Evaluation. *Int. J. Heat and Fluid Flow* 30(1), 131–39.

Heun, M. K., & Dunn, W. E. (1995). *Performance and optimization of microchannel condensers*. ACRC Report TR 81. Air Conditioning and Refrigeration Center. University of Illinois at Urbana-Champaign.

Huang, L., Aute, V., & Radermacher, R. (2015). Airflow distribution and design optimization of variable geometry microchannel heat exchangers. *Science and Technology for the Built Environment*, *21*(5), 693-702.

Kulkarni, T., Kim, M. H., & Bullard, C. W. (2001). *Condensing Units for Household Refrigerator-Freezers*. ACRC Report CR 38. Air Conditioning and Refrigeration Center. University of Illinois at Urbana-Champaign.

Li, J., & Hrnjak, P. (2016). Separation of Liquid and Vapor in Header of MCHE. International Refrigeration and Air Conditioning Conference. Paper 1667.

Li, J & Hrnjak, P. (2017a). Separation in Condensers as a Way to Improve Efficiency. *Int. J. Refrig.*, 79, 1–9.

Li, J & Hrnjak, P. (2017b). Improvement of Condenser Performance by Phase Separation Confirmed Experimentally and by Modeling. *Int. J. Refrig.*, 78, 60–69.

Li, J & Hrnjak, P. (2018). An experimentally validated model for microchannel condensers with separation circuiting. *17th International Refrigeration and Air Conditioning Conference*, in review. West Lafayette, IN: Purdue.

Martínez-Ballester, S., Corberán, J. M., & Gonzálvez-Maciá, J. (2013). Numerical model for microchannel condensers and gas coolers: Part II–Simulation studies and model comparison. *International J. Refrig., 36*(1), 191-202.

SAE International, 2008, Procedure for Measuring System COP [Coefficient of Performance] of a Mobile Air Conditioning System on a Test Bench, SAE Surface Vehicle Standard J2765 OCT2008, Atlanta GA.

ACKNOWLEDGEMENT

The authors thankfully acknowledge the support provided by the Air Conditioning and Refrigeration Center at the University of Illinois at Urbana-Champaign.